Journal of Poultry Sciences and Avian Diseases

Journal homepage: www.jpsad.com

CT Anatomy and Gross Anatomical Study of the Scleral Ring in the Common Buzzard (Buteo buteo)

Majid Masoudifard[1], Omid Zehtabvar[2*], Yasaman Rezvani[3], Shayan Zand[1], Arman Shahbazi[3]

[1] Department of Surgery and Radiology, Faculty of Veterinary Medicine, University of Tehran, Tehran, Iran
[2] Department of Basic Sciences, Faculty of Veterinary Medicine, University of Tehran, Tehran, Iran
[3] Faculty of Veterinary Medicine, University of Tehran, Tehran, Iran

*** Corresponding author email address**: ozehtabvar@ut.ac.ir

A r t i c l e I n f o

Article type:
Original Research

How to cite this article:
Masoudifard, M., Zehtabvar, O., Rezvani, Y., Zand, S., & Shahbazi, A. (2026). CT Anatomy and Gross Anatomical Study of the Scleral Ring in the Common Buzzard (Buteo buteo). *Journal of Poultry Sciences and Avian Diseases*, *4*(1), 1-12.
http://dx.doi.org/10.61838/kman.jpsad.139

A B S T R A C T

The avian scleral ring is a critical structure for ocular biomechanics and taxonomic studies, yet its morphology in raptors remains understudied. This study investigated the scleral ring in the common buzzard (Buteo buteo) using a multimodal approach: CT, micro-CT, radiography, and anatomical dissection. Analysis of five adult specimens revealed a semi-hyperbolic ring composed of 15 quadrilateral ossicles arranged in a Type B pattern (one plus and one minus excellent ossicle), with a mean anterior-posterior to width ratio of 1.32. Micro-CT imaging showed that 53.36%±1.89 of each ossicle's volume was compact bone, suggesting biomechanical reinforcement against flight-induced stresses. The ring exhibited complete anatomical independence from adjacent cranial bones (frontal, jugal, lacrimal) and perfect bilateral symmetry ($p>0.05$). High-resolution micro-CT scans resolved microscopic articular interfaces and trabecular architecture non-destructively, validating its utility for delicate orbital studies. These findings provide morphometric benchmarks for comparative anatomy in Accipitriformes, demonstrate the efficacy of non-invasive imaging for species differentiation, and offer diagnostic criteria for ocular trauma management. By integrating macroscopic dissection with advanced tomography, this work establishes a framework for evolutionary, clinical, and conservation-focused studies of avian visual systems.

Keywords: *Anatomy, Avian Vision, Common Buzzard, Computed Tomography, Ossicle, Scleral Ring*

1 Introduction

The Common Buzzard (*Buteo buteo*) is a medium-sized raptor belonging to the order *Accipitriformes* and the family *Accipitridae* (1). The avian ocular globe shares a fundamental structural similarity with mammals; however, the eye occupies a larger proportion of the cranial volume compared to mammals (2). While the overall shape of the eye is globular, interspecific variations -particularly in the anterior segment of the ocular globe- were observed. In most

Article history:
Received 31 May 2025
Revised 14 July 2025
Accepted 22 August 2025
Published online 01 January 2026

avian species, the eye extensively fills the orbital cavity and exhibits limited mobility (3). Notably, in many birds, the combined mass of the eyes exceeds that of the brain (2).

In birds, the cornea exhibits a relatively small diameter but is highly convex, while the ocular globe has a significantly larger diameter (3). In owls and eagles, the cornea is notably broader and more arched compared to other avian species (2). The scleral ring, a structure located in the eye, forms an intermediate zone between the anterior segment (housing the cornea) and the posterior segment of the ocular globe, which occupies a substantial volume. In owls, this intermediate region is elongated, contributing to the tubular appearance of the anterior eye, a characteristic often described as "tubular-shaped" (2).

The sclerotic bone ring is not exclusive to birds; it is also observed in many reptiles (2). Two primary functions have been proposed for this osseous structure: first, it prevents deformation of the ocular globe during flight or diving, and second, it aids the function of the ciliary muscles, playing a role in accommodation. Beyond these primary functions, the scleral ring has been suggested to influence binocular vision by enabling the animal to modify the shape of the cornea, thereby altering its refractive power. This capability has not yet been thoroughly studied across all animal taxa possessing this structure (4).

In reptiles, the number of ossicles in the scleral ring is fewer compared to birds (5). A 2008 study noted that these ossicles are dermal bones in avian (6).

The scleral ossicles in penguins exhibit unique articular facets that form overlapping bony plates, creating a double-walled structure. As demonstrated in Magellanic penguins (7), these facets cover approximately one-third of each ossicle's surface, providing exceptional mechanical stability to the ocular ring during diving (7).

The morphology, number, and arrangement of sclerotic ossicles vary significantly across different animal groups. In many birds, the ossicles are quadrilateral in shape, while in others, they are somewhat elongated and concave. In birds, each scleral ring typically consists of 10 to 18 ossicles (2).

The ossicles within the ring are classified based on the articular surfaces they form with adjacent ossicles. Ossicles that alter the sequence and rhythm of overlapping articular surfaces are termed excellent ossicles, while the others are referred to as interlocked ossicles. excellent ossicles are further divided into two types: plus and minus. A plus excellent ossicle overlaps both articular surfaces of its neighboring ossicles, whereas a minus excellent ossicle is overlapped by both neighboring ossicles on its articular surfaces. An interlocked ossicle overlaps one neighboring ossicle on one side and is overlapped by another on the opposite side (8). Based on the number of excellent ossicles present in the ring, two types of rings are identified: Type A, which contains four excellent ossicles, and Type B, which contains two excellent ossicles (8). To count the ossicles within the ring, we begin with an excellent ossicle located on the ventral side of the ring, which is designated as ossicle number one. From there, counting proceeds laterally—clockwise in the right eye and counterclockwise in the left eye (9).

The overall morphology of the scleral ring, including the number and shape of its ossicles, their arrangement, and the presence of any processes, serves as a valuable characteristic for taxonomic classification. Given the general structure of the scleral ring in buzzards (*Buteo* spp.) and its similarities and differences compared to other species, this feature can be utilized for more precise classification. Furthermore, a detailed understanding of the position and structure of the scleral ring is crucial for effectively treating injuries and fractures, particularly in cases involving trauma to the cranial and ocular regions. It should be noted that the morphometric information presented in this study has not been mentioned in other sources on this species of bird of prey, and a key objective of this study was to present this morphometric information. In addition, one of the hypotheses examined in this study is the similarity of the structure of the scleral ring in this species of bird with that of other species.

2 Materials and methods

Samples: For this study, five adult common buzzards (*Buteo buteo*), with an average weight of 950 grams, were examined. It is important to note that these specimens were selected from cases where euthanasia had been deemed necessary due to various health issues unrelated to ocular conditions. Regarding the number of samples studied, it should be noted that the minimum acceptable number for anatomical studies was selected to be statistically similar to other articles on this topic, which of course did not create any specific limitations, but, if possible, it would have been better to select male and female samples so that comparisons between males and females could be made.

CT Scan Studies: In this study, a Siemens Somatom Spirit 2 CT scanner was used. Initially, the buzzards were anesthetized using a combination of ketamine (5 mg/kg body weight), medetomidine (40 µg/kg body weight), and

butorphanol (1 mg/kg body weight) (10). The drugs were administered intramuscularly into the pectoral muscle. For the CT scan, the specimens were positioned prone on the scanner table.

Technical Parameters of the CT Scan: Rotation time, 1s; slice thickness, 1mm; reconstruction interval, 0.5–1 mm; pitch, 1; X-ray tube potential, 120 kV; and X-ray tube current, 130 mAs.

Radiographic Studies: In this study, a Kodak DirectView CR 850 digital radiography system was used. Radiographs were acquired in the dorsoventral projection, with the following technical parameters: 4 mAs and 45 kVp.

Micro CT scan studies: For this stage, the bodies of five adult common buzzards collected from veterinary centers in Tehran were used. The causes of death of these birds were due to events unrelated to the head and eyeball area. The ocular globe was meticulously excised from the cranial cavity and subsequently prepared for examination via micro-computed tomography (micro CT) scanning. In this study, we employed an in vivo micro CT scanner (LOTUS inVivo, Behin Negareh Co., Tehran, Iran) located within the Preclinical Core Facility (TPCF) at Tehran University of Medical Sciences. The LOTUS-inVivo apparatus is equipped with a cone beam micro-focus X-ray source in conjunction with a flat panel detector. To ensure optimal image fidelity, the X-ray tube voltage and current were calibrated to 70 kV and 70 µA, respectively, while the frame exposure time was established at 1 second per 3-fold magnification. The comprehensive duration for the scanning process was 30 minutes. The slice thickness of the reconstructed images was configured to 25 µm. The LOTUS-invivo-ACQ software oversaw the entirety of the procedural configurations. The resultant three-dimensional dataset was reconstructed utilizing LOTUS inVivo-REC through the implementation of a standardized Feldkamp, Davis, Kress (FDK) algorithm.

Dissection and Anatomical Studies: The same five cadavers used for the micro-CT scans were used in this step. Based on the data obtained in the previous stage and existing information from other avian species, anatomical dissection and examinations were conducted. After isolating the head region of the specimens, the skin was removed. The skeletal structures were then isolated using an insect-based maceration method over one week (a temperature of 27°C and relative humidity of 70% were maintained to ensure optimal skeletal preparation by the insects). For further examination and imaging, an Olympus SZX12 stereo microscope equipped with a digital camera (ASP-CellPad E) was used.

Morphometric studies: Morphometric measurements were performed using the Syngo MMWP VE40A software available in the CT scan device. Measurements were performed on CT scan images. The Independent t-test and the paired t-test were employed to conduct a comprehensive analysis of the data. $p \leq 0.05$ was considered statistically significant.

The description of the measured parameters is as follows:

- **Anterior Scleral Ring Diameter**: The transverse width of the scleral ring's anterior segment was quantified using 3D CT reconstructions, measuring the maximum horizontal span across the ring's frontal aspect.
- **Posterior Scleral Ring Diameter**: The maximum horizontal width of the ring's posterior segment was determined through volumetric CT analysis, capturing the transverse dimension at the structure's caudal termination.
- **Axial Scleral Ring Length**: Linear measurements along the horizontal plane were obtained to determine the anteroposterior span between the ring's most rostral and caudal margins using multiplanar CT reconstruction.
- **Skull Length Measurement**: Three-dimensional CT datasets enabled quantification of the skull's maximum longitudinal dimension, measured between the most prominent anterior and posterior osseous landmarks.
- **Skull Height Measurement**: The vertical skull dimension was assessed by measuring the greatest dorsoventral distance between the cranial vault's superior and inferior boundaries in reconstructed CT images.
- **Skull Width Measurement**: Transverse skull proportions were evaluated by measuring the maximal bilateral distance between the left and right lateral surfaces in 3D rendered CT volumes.
- **Orbital Diameter**: Maximum intercanthal distance was measured in coronal CT planes, representing the transverse span between the medial and lateral orbital margins.
- **Orbital Depth**: Anteroposterior orbital dimension was quantified in sagittal CT reconstructions, measuring from the orbital rim to the optic foramen along the visual axis.

- **Optic Nerve Length**: The intracranial course of the optic nerve was traced in multiplanar CT reconstructions, with measurements obtained from the optic disc to the chiasmal junction.
- **Optic Nerve Sheath Diameter (ONSD)**: Perineural subarachnoid space dimensions were assessed at 3mm posterior to the globe in axial CT images, using standardized caliper placement protocols.
- **Tissue Volumetrics**
- Using Syngo MMWP VE40A software, we performed:
- **Ocular Volume:** Segmentation of globe contours in all three planes (coronal, sagittal, axial)
- **Lens Volume:** Threshold-based isolation of lenticular structures
- **Brain Volume:** Whole-brain volumetry excluding cranial nerves and meninges
- **Chamber Volumetrics**
- The software's advanced segmentation algorithms calculated:
- **Vitreous Chamber Volume:** Automated differentiation from retinal layers
- **Anterior/Posterior Chamber Volumes:** Boundary detection at corneal endothelium and iris plane (11).

3 Results

In the radiographic images, the structure of the scleral ring was visible due to its osseous opacity in both dorsoventral (DV) and lateral views. However, in the lateral view, the overlapping cranial structures made it difficult to fully examine the scleral ring, whereas the dorsoventral view provided a clearer and more isolated visualization of this structure. The lack of connection between the scleral ring and other cranial regions was particularly evident in the dorsoventral view (Figure 1).

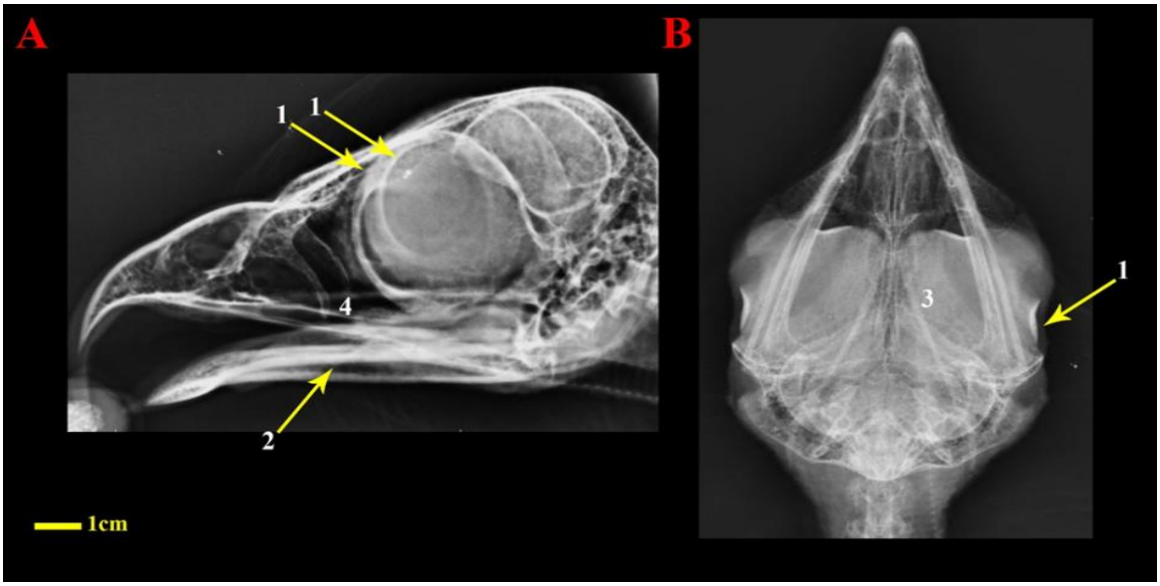

Figure 1. Lateral (A) and Dorsoventral (B) Radiographs of the Head Region in the Common Buzzard (Buteo buteo). 1. Scleral ring 2. Mandible 3. Hyobranchial apparatus (ceratobranchiale) 4. Jugal bone

In the three-dimensional (3D) reconstructed CT images, the osseous appearance of the scleral ring was visible. In these images, the boundaries between the ossicles were partially discernible. Additionally, the proximity of this structure to the frontal bone, jugal bone, and lacrimal bone was observed. The ring exhibited a semi-hyperbolic and relatively rounded morphology, which was visible and assessable in the 3D images (Figure 2 and Figure 3).

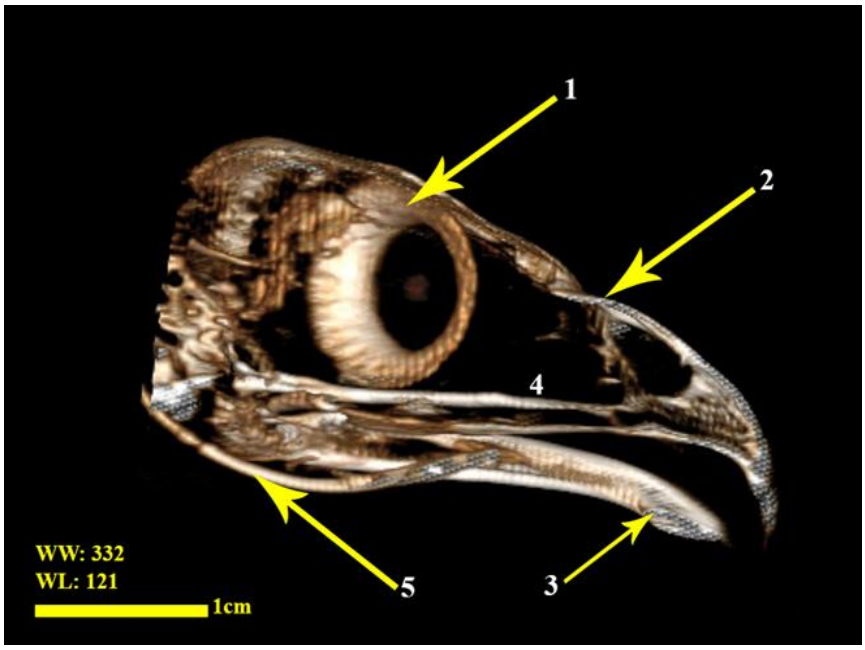

Figure 2. Medial View of a Sagittal 3D CT Scan Reconstruction of the Head Region in the Common Buzzard (Osseous-Shaded-vp Rendering).

1. Scleral ring, 2. Nasal bone, 3. Mandible, 4. Jugal bone, 5. Hyobranchial apparatus (ceratobranchiale).

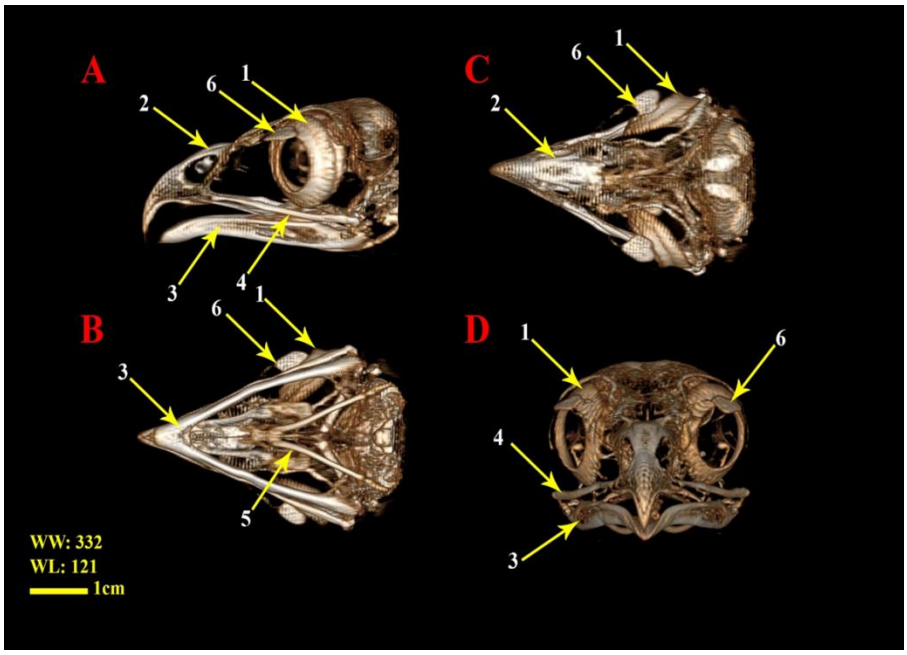

Figure 3. 3D CT Scan Reconstruction of the Head Region in Buteo buteo (Osseous-Shaded-vp Rendering).

A: Lateral View B: Ventral View C: Dorsal View D: Anterior View

1. Scleral ring, 2. Nasal bone, 3. Mandible, 4. Jugal bone, 5. Hyobranchial apparatus, 6. Lacrimal bone.

In the two-dimensional (2D) transverse CT images, moving from the cranial to the caudal direction, the structure of the scleral ring was examined. Initially, the ring appeared as two separate linear structures at the superior and inferior aspects of the ocular globe. As we moved toward the center, the crescent-shaped morphology of the ring became more distinct and prominent. The proximity and lack of connection to other cranial bones were evaluable in this view. Furthermore, since the images were acquired while the animal was alive, soft tissues were visible, allowing clear

visualization of the lens's proximity to the anterior, tubular portion of the scleral ring (Figure 4).

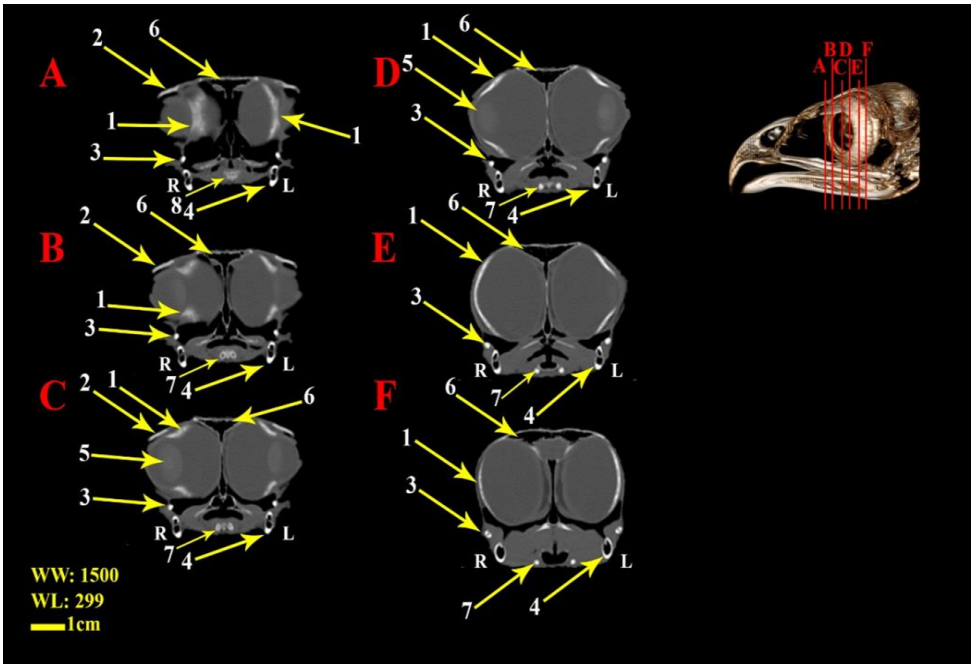

Figure 4. Two-dimensional transverse CT scan images of the head area in Buteo buteo, the cross-section of each transverse image is specified in the three-dimensional image. 1. Scleral ring, 2. Lacrimal bone, 3. Jugal bone, 4. Mandible, 5. Lens, 6. Frontal sinus, 7. Hyobranchial apparatus, 8. Hyobranchial apparatus.

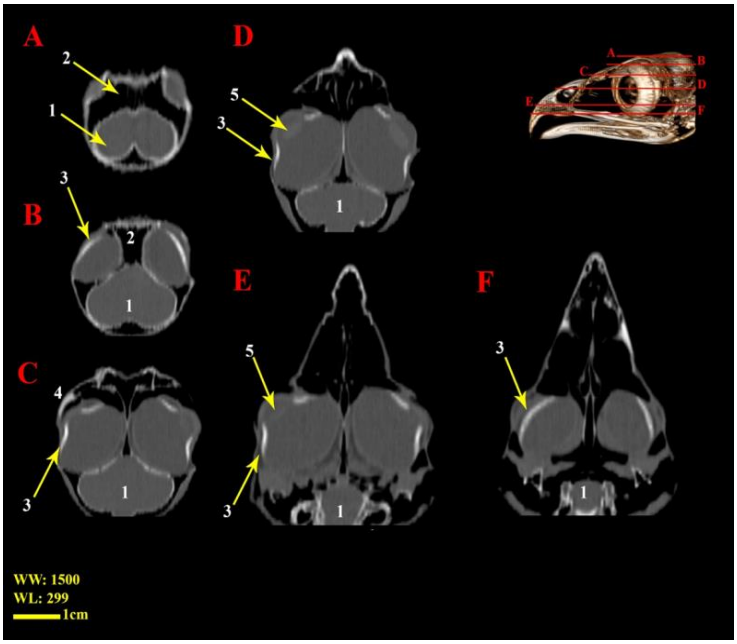

Figure 5. Longitudinal (sagittal) two-dimensional CT scan images (bone window) of the head area in Buteo buteo, the cross-section of each of the transverse images is specified in the three-dimensional image.

Brain, 2. Frontal sinus, 3. Scleral ring, 4. Lacrimal bone, 5. Lens

In the 2D longitudinal (sagittal or dorsal) CT images, the osseous structure was also clearly visible, similar to the

transverse view. However, the transverse images provided a better assessment of the ring's proximity and lack of connection to other cranial bones (Figure 5).

Micro-CT scan images reveal the spatial arrangement pattern of the ossicles within the scleral ring, with the excellent ossicles being distinguishable (Figure 6). In two-dimensional micro-CT scan images, the articular surfaces between adjacent ossicles can be observed, along with the ability to quantify the trabecular or compact bone density of each ossicle (Figure 7).

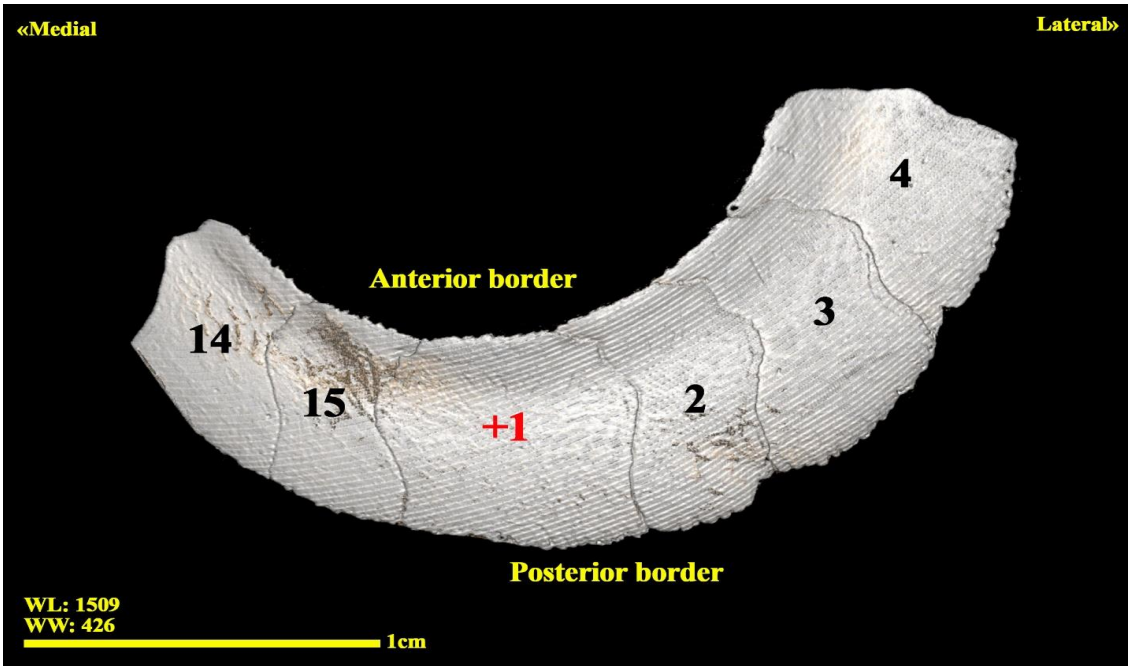

Figure 6. Micro-CT three-dimensional reconstructed image of the left scleral ring (External surface, anterior view) of the Common Buzzard (Buteo buteo)

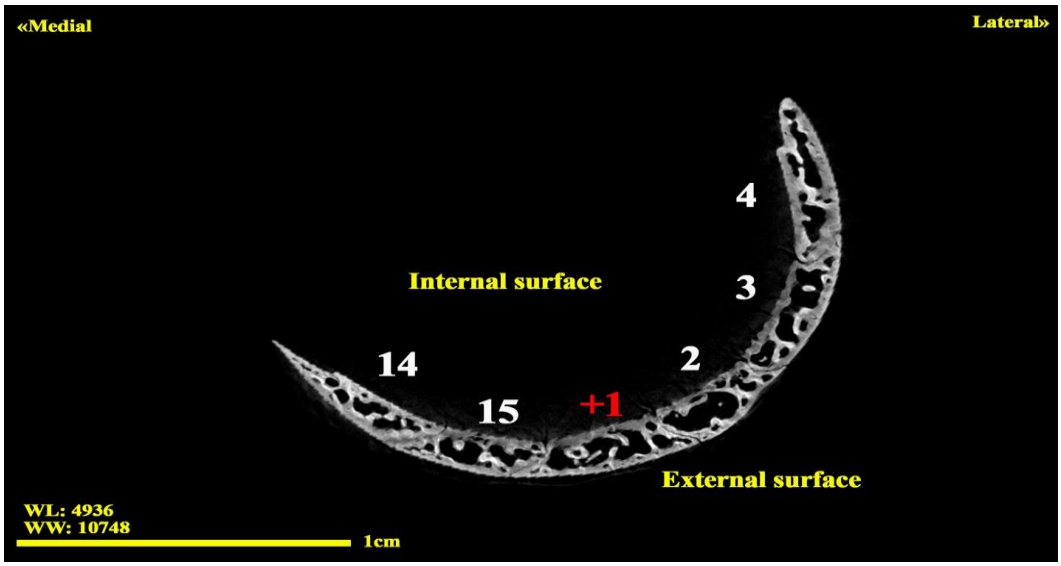

Figure 7. Micro-CT two-dimensional transverse image of the left scleral ring (External surface, anterior view) of the Common Buzzard (Buteo buteo)

In the anatomical examination of the scleral ring in the Common Buzzard (*Buteo buteo*), this structure exhibited a semi-hyperbolic or volcano-shaped morphology (Figure 8). The anterior portion of the ring was shorter than the posterior portion (Figure 8). The scleral ring was relatively rounded, with no distinct poles at its external or internal base. Two

diameters were defined for the base of the structure: a horizontal diameter and a vertical diameter. These two diameters were approximately equal. The internal wall of the ring was shorter than the lateral wall. The semi-hyperbolic structure of the scleral ring featured two rims—an anterior rim and a posterior rim. The circumference of the anterior rim was smaller than that of the posterior rim, with the posterior rim corresponding to the base of the ring. Both the anterior and posterior rims were nearly circular (Figure 8). Additionally, both rims were relatively smooth, and no articular connections or joints were observed between the scleral ring and other cranial skeletal structures. Overall, the scleral ring comprised a tubular anterior segment and a flared, funnel-shaped posterior segment (Figure 8).

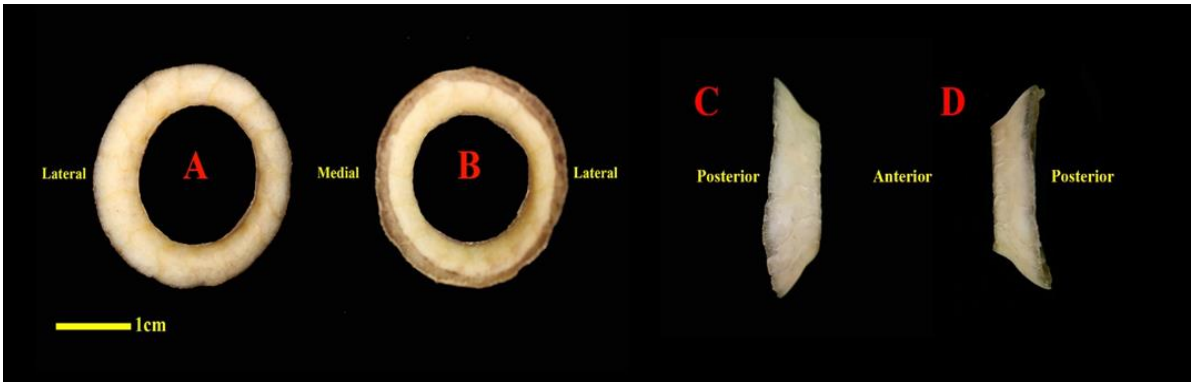

Figure 8. Anatomical samples of the scleral ring in Buteo buteo,

A: Anterior view, B: Posterior view, C: Lateral view, D: Medial view

Figure 9. Anatomical samples of scleral ossicles in Buteo buteo, A and C: External surface, B and D: Internal surface. 1. Articular surface, 2. Articulation between two ossicles.

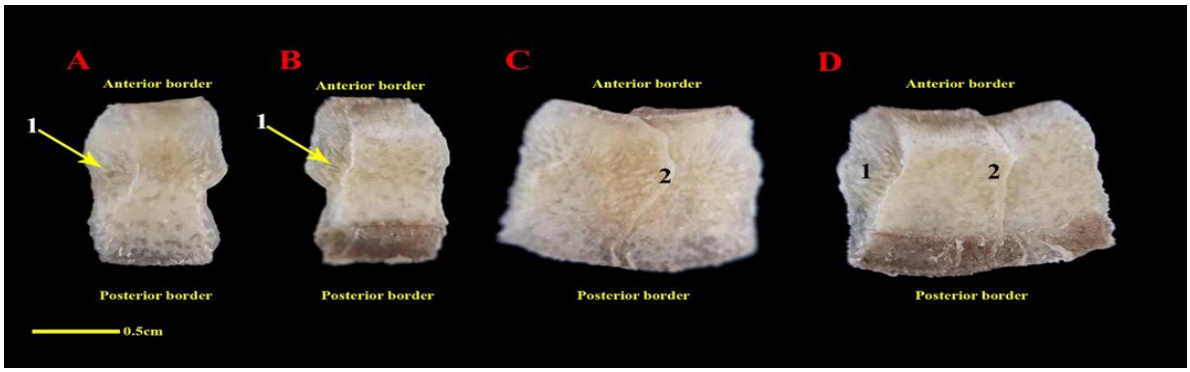

The scleral ring in all specimens consisted of 15 ossicles (Figure 4). These ossicles exhibited a quadrilateral structure. The internal surface of each ossicle was convex, while the external surface was concave (Figure 9). Each ossicle had four sides, with a rectangular appearance. The longer sides of ossicles articulated with other ossicles, while the shorter sides contributed to the formation of the anterior and posterior rims of the scleral ring. Each ossicle was thicker at its center compared to its edges. The longer sides of the segments, which articulated with neighboring ossicles, featured articular surfaces for interfacing with adjacent ossicles. At these articular surfaces, the bone was recessed at a fixed angle, allowing the segments to align and form a continuous ring-like structure (Figure 9).

In all specimens, a plus excellent ossicle was located in the ventral position of the scleral rings and was named as Ossicle number 1. Subsequent numbering of the ossicles proceeded laterally (clockwise in the right eye and counterclockwise in the left eye). Ossicle number 5 was consistently a minus excellent ossicle situated in the temporal position of rings, while the remaining ossicles were of the interlocked type.

In the morphometric results, as shown in Table 1 and Table 2, there was no statistically significant difference between the measured parameters of the right and left sides (p<0.05).

Table 1. Measured Parameters of the Scleral Ring and Skull in the Common Buzzard (cm)

Parameters	Mean±SD (Right eye)	Mean±SD (Left eye)
Anterior diameter (Scleral ring)	1.63±0.23[a]	1.57±0.41[a]
Axial scleral ring length	0.59±0.24[b]	0.57±0.314[b]
Posterior diameter (Scleral ring)	2.51±0.32[c]	2.57±0.22[c]
Orbit diameter	3.43±0.45[d]	3.33±0.24[d]
Orbit depth	3.16±0.21[e]	3.25±0.34[e]
Skull length	8.49±0.37	
Skull height	4.21±0.32	
Skull width	5.19±0.24	
Optic nerve length	0.55±0.01[f]	0.55±0.01f
Optic nerve sheath diameter	0.42±0.01[g]	0.41±0.01[g]

The heterogeneous letters in each row indicate statistically significant differences between the right and left parameters (p<0.05).

Table 2. Measured volumes of the eyeballs and brain of the Common Buzzard (Buteo buteo). (cm3)

Parameter	Right eye Mean±SD	Left eye Mean±SD
Volume of the eyeball	23.42±1.3[a]	21.6±0.99[a]
Volume of the anterior and posterior chamber	4.58±0.12[b]	4.5±0.11[b]
Volume of the Lens	0.83±0.2[c]	0.81±0.09[c]
Volume of the vitreous chamber	18.45±0.93[d]	18.7±0.96[d]
Volume of the brain	27.5±1.41	

The heterogeneous letters indicate statistically significant differences between the right and left parameters (p<0.05).

Through the quantification of the thickness, length, and width of the ossicular components of the scleral ring, it was ascertained that the excellent plus and minus and interlocking ossicles exhibit no statistically significant variations in dimensions (p>0.05). The average length (AP) to width ratio of each ossicle is 1.32 (Table 3).

Table 3. Measured parameters of the ossicles of the Common Buzzard (Buteo buteo). (mm)

Parameters	Width	Length (AP)	Thickness
Mean±SD ossicles	5.82±0.29	7.71±0.13	0.73±0.04

The comparative analysis of the ratio of eye volume to brain volume was also conducted. In this study, it was discerned that in *Buteo buteo*, the brain volume exceeds that of a single eye, while the cumulative volume of both eyes surpasses that of the brain.

Micro CT imaging analysis demonstrated that approximately 53.36%±1.89 of the osseous tissue constituting each ossicle is comprised of compact bone, whereas 46.64%±1.89 is identified as cancellous (spongy) bone (Table 4).

Table 4. Measured volumes of the ossicles of the Common Buzzard (Buteo buteo).

Parameters	Volume (cm^3)	Percentage
Total ossicle	$(1.05\pm0.02)\times10^{-4}$	100 %
Spongy ossicle	$(0.49\pm0.02)\times10^{-4}$	46.64±1.89 %
Cortical ossicle	$(0.56\pm0.02)\times10^{-4}$	53.36±1.89 %

4 Discussion

The overall morphology of the scleral ring and its constituent ossicles is a valuable characteristic for taxonomic classification. Lima et al. investigated the structure of sclerotic ossicles in Brazilian birds. In their study, 208 birds from 18 different orders were examined. The number of sclerotic ossicles varied between species, ranging from 11 to 16. The study also noted that the number of ossicles in each eye of *Rupornis magnirostris* and *Geranoaetus albicaudatus* is 15. Similarly, in the current study on the Common Buzzard (*Buteo buteo*), the same number of ossicles (15) was observed (4), given the lack of

statistically significant differences between the right and left parameters in adult buzzards.

It has been noted that in the orders Accipitriformes, Strigiformes (owls), and aquatic birds, the elliptical shape of the ocular globe influences the morphology of the sclerotic ossicles, resulting in a tubular-shaped eye. This adaptation prevents deformation of the ocular globe under varying water and air pressures (2).

According to reports by Hall, the scleral papillae induce the formation of sclerotic ossicles, and there is always a precise correlation between the number of ossicles and the papillae (12). Hall and Miyake explain that the scleral papillae undergo intramembranous ossification in reptiles and birds; ossification occurs through endochondral ossification (13).

The morphology, number, and distribution of sclerotic ossicles vary significantly across different animal groups. In most birds, the ossicles are rectangular, while in some species, they are slightly elongated and concave. However, the precise pattern of these ossicles remains unclear in many animals, and advancing this knowledge would be highly beneficial for various clinical and therapeutic applications (4).

In high-speed flying birds such as members of the orders Accipitriformes (hawks and eagles) and Strigiformes (owls), the elliptical shape of the ocular globe influences the morphology of the sclerotic ossicles, elongating them. In owls, in addition to elongation, the concavity of the ossicles confers a tubular shape to the eye. This osseous system stabilizes the ocular globe against deformation during flight or aquatic dives, while also enhancing visual acuity and providing structural support and protection (14).

Andrews reported that in turtles, sclerotic ossicles develop through endochondral ossification, while in birds, they develop through intramembranous ossification following a complex epithelial-mesenchymal induction process (15).

There are reports of fractures in this osseous structure in various bird species due to trauma to the head, along with diagnostic methods for identifying such injuries. Denis et al. documented the diagnosis of a fracture in the scleral ring of a Red-tailed Hawk (*Buteo jamaicensis*) using radiography. Additionally, Schmitz conducted a quantitative study on the osseous structures associated with vision in fossilized birds to estimate their visual capabilities (16).

In Accipitriformes, the ossicles are square or rectangular; in Psittaciformes, Columbiformes, and Gruiformes, they are trapezoidal; and in Piciformes, they are irregular with sinusoidal edges. In reptiles, the ossicles are typically flat, although they may often be slightly curved. Their organization around the sclera results in overlapping ossicles in most species. In some cases, where the edges of these plates are in contact, they form a continuous structure, while in others, they are arranged in a distinct pattern. This overlapping provides an adaptive advantage, allowing the structure to expand and contract for ocular accommodation (17, 18).

This additional support represents an adaptive advantage, particularly when the eyes are exposed to intense hydrodynamic pressures or aerodynamic forces during flight. According to Curtis and Miller, the sclerotic ossicles and cartilages also contribute to pupil regulation and the function of ciliary muscles involved in visual accommodation (19).

In 1998, morphological, anatomical, and histological studies were conducted on 10 owl species, with results compared to other species such as the Common Potoo (*Nyctibius griseus*) and the Domestic Duck (*Anas platyrhynchos*). The analysis revealed that in owls and potoos, the *nictitating membrane* (third eyelid) is located at the anterior margin of the eye. Additionally, these birds possess an accessory ossification within the scleral ring, termed the scleral sesamoid bone, which varies in size. This bone lies along the tendon of the *pyramidal muscle* and features a groove to accommodate it. The structure prevents detachment of the muscle from the sclera during contraction and stabilizes the tendon during muscle activity. The pyramidal muscle is also linked to the nictitating membrane, which in owls is positioned at the dorsal margin of the ocular globe. The term "scleral sesamoid bone" was proposed for this structure (20). In our study on the Common Buzzard (*Buteo buteo*), no such accessory bony structure separate from the scleral ring was observed.

In the study by Bohórquez, it was noted that the distinctive scleral sesamoid bone was not observed in *Glaucidium brasilianum*. However, in *Athene cunicularia*, a small, rounded structure was identified; in *Bubo bubo*, an elongated structure; and *Bubo virginianus*, an elongated, bifurcated structure (20). In contrast, none of these three morphological variants were observed in our study species, *Buteo buteo*. Given the high-resolution radiographic and CT imaging (2D and 3D reconstructions) with a 1mm slice thickness, the likelihood of missing such a bone due to procedural errors during skeletal isolation is negligible. If a structure of the size reported in Mahecha's study

(approximately 3mm) had been present, it would have been detectable in our imaging protocols.

Hadden et al. investigated the scleral rings of various species of penguins using micro CT imaging techniques and discovered that in *Pygoscelis papua* chicks, the volume of spongy bone tissue present in the ossicles is significantly greater than that observed in adult specimens. In our study, more than 50% of the volume of each ossicle was composed of compact bone (21).

Zehtabvar et al. conducted a comprehensive investigation into the structure of the scleral ring within the species *Asio otus*, yielding results that indicate a symmetrical configuration of the scleral ring in both the right and left ocular organs concerning shape, dimensionality, and the quantity of osseous components comprising the ring. This particular anatomical formation is constituted of 15 ossicles, all samples are type B, and the analysis revealed no statistically significant disparities among the parameters evaluated in the left and right ocular organs; nevertheless, the majority of ocular parameters assessed in female specimens were observed to be greater than those in male specimens, notably including the measurement of the eyeball's size (22).

While our study of *Buteo buteo* revealed a consistent Type B scleral ring with 15 ossicles (53.36% compact bone), ostrich specimens (*Struthio camelus*) exhibited greater variability (15-17 ossicles) with a Type A pattern and higher compact bone content (67.26%). Crucially, the length-to-width ratio of ossicles differed significantly: *Buteo buteo* showed a ratio of 1.32 (AP length/width), whereas ostrich ossicles displayed an inverse width-to-length ratio of 1.44 (9.64±0.26 mm width / 6.11±0.007 mm length) (11).

Given the general structure of the scleral ring in *Buteo* spp. and its similarities and differences compared to other species, this feature can be utilized for more precise taxonomic classification. Furthermore, our study demonstrates that radiographic and CT imaging techniques, when cross-validated with necropsy findings, enable high-precision in vivo evaluation of this structure. This non-invasive approach is particularly advantageous for detecting anatomical anomalies or classifying rare species where euthanasia and necropsy are logistically or ethically prohibitive. Additionally, detailed knowledge of the scleral ring’s position and architecture is critical for optimizing treatment strategies for cranial and ocular injuries, such as fractures or trauma, which commonly affect this region.

5 Conclusion

This study elucidates the intricate anatomy of the scleral ring in *Buteo buteo* through a multidisciplinary approach combining advanced imaging techniques and anatomical dissection. The ring's semi-hyperbolic structure, composed of 15 quadrilateral ossicles arranged in a Type B pattern (featuring two excellent ossicles: one *plus* and one *minus*), demonstrates remarkable symmetry and biomechanical specialization. The predominance of compact bone (53.36%±1.89) in the ossicular composition suggests an adaptive reinforcement against the stresses of flight, while the absence of articular connections to adjacent cranial structures highlights its functional autonomy. These findings not only provide a baseline for comparative studies in raptors but also validate the efficacy of non-invasive imaging for detailed morphological analysis.

The Type B configuration, observed here and in related species, emerges as a potential taxonomic marker within *Accipitriformes*. The consistent ossicle count and arrangement across specimens, coupled with the ring's distinct spatial relationship to ocular and cranial elements, offer diagnostic criteria for species identification and phylogenetic studies. Furthermore, the successful application of CT and micro CT imaging underscores their utility in veterinary and conservation contexts, particularly for protected species where traditional dissection is impractical. Another thing to consider in the future is the comparison of the characteristics of the scleral ring in male and female birds.

Acknowledgements

The authors wish to express their appreciation to everyone who assisted in this study.

Conflict of Interest

The authors declare no competing interests.

Author Contributions

All authors equally contributed to this study.

Data Availability Statement

The data that support the findings of this study are available from the corresponding author upon reasonable request.

Ethical Considerations

This study was a DVM thesis, Faculty of Veterinary Medicine, University of Tehran (ID: 3815).

Funding

No funding was received for this research.

References

1. Ferguson-Lees J, Christie D, Franklin K, Mead D, Burton P. Raptors of the world Houghton Mifflin Company. Boston, Massachusetts. 2001.
2. King A, McLelland J. Birds, their structure and function. 1984.
3. Dyce KM, Sack WO, Wensing CJG. Textbook of veterinary anatomy-E-Book: Elsevier Health Sciences; 2009. 3_https://doi.org/DOI}
4. Lima FC, Vieira L, Santos A, De Simone S, Hirano L, Silva J, et al. Anatomy of the scleral ossicles in Brazilian birds. Journal of Morphological Sciences. 2017;26(3-4):0-.
5. Franz-Odendaal TA, Vickaryous MK. Skeletal elements in the vertebrate eye and adnexa: Morphological and developmental perspectives. Developmental dynamics: an official publication of the American Association of Anatomists. 2006;235(5):1244-55. [PMID: 16496288] [DOI]
6. Franz-Odendaal TA. Scleral ossicles of teleostei: evolutionary and developmental trends. The Anatomical Record: Advances in Integrative Anatomy and Evolutionary Biology: Advances in Integrative Anatomy and Evolutionary Biology. 2008;291(2):161-8. [PMID: 18213703] [DOI]
7. Suburo AM, Scolaro JA. The eye of the magellanic penguin (Spheniscus magellanicus): structure of the anterior segment. American journal of anatomy. 1990;189(3):245-52. [PMID: 2260531] [DOI]
8. Fischer O, Schoenemann B. Why are bones in vertebrate eyes? Morphology, development and function of scleral ossicles in vertebrate eyes—A comparative study. J Anat Physiol Stud. 2019;3:1-26.
9. Lemmrich W. Der skleralring der vögel: Fischer; 1931. 3_https://doi.org/DOI}
10. Carpenter JW, Marion C. Exotic Animal Formulary-E-Book: Exotic Animal Formulary-E-Book: Elsevier health sciences; 2017. 3_https://doi.org/DOI}
11. Masoudifard M, Zehtabvar O, Shahbazi A, Raad SB, Tonekabony SHM. Anatomical Study of the Scleral Ring and Scleral Ossicles of the Ostrich (Struthio camelus) With Gross Anatomical Methods and Diagnostic Imaging Techniques. Veterinary Medicine International. 2025;2025(1):4993179. [PMID: 40662086] [PMCID: PMC12256172] [DOI]
12. Hall BK. Specificity in the differentiation and morphogenesis of neural crest-derived scleral ossicles and of epithelial scleral papillae in the eye of the embryonic chick. Development. 1981;66(1):175-90. [DOI]
13. Hall BK, Miyake T. Divide, accumulate, differentiate: cell condensation in skeletal development revisited. International Journal of Developmental Biology. 1995;39:881-94.
14. Romer A. Osteology of the reptiles university of chicago press. Chicago, Illinois. 1956.
15. Andrews KD. An endochondral rather than a dermal origin for scleral ossicles in Cryptodiran turtles. Journal of Herpetology. 1996;30(2):257-60. [DOI]
16. Schmitz L. Quantitative estimates of visual performance features in fossil birds. Journal of Morphology. 2009;270(6):759-73. [PMID: 19123246] [DOI]
17. Franz-Odendaal TA, Hall BK. Skeletal elements within teleost eyes and a discussion of their homology. Journal of Morphology. 2006;267(11):1326-37. [PMID: 17051547] [DOI]
18. Hall M, Ross C. Eye shape and activity pattern in birds. Journal of Zoology. 2007;271(4):437-44. [DOI]
19. Curtis EL, Miller RC. The sclerotic ring in North American birds. The Auk. 1938;55(2):225-43. [DOI]
20. Bohórquez Mahecha G, Aparecida de Oliveira C. An additional bone in the sclera of the eyes of owls and the common potoo (Nictibius griseus) and its role in the contraction of the nictitating membrane. Acta Anatomica. 1998;163(4):201-11. [PMID: 10072568] [DOI]
21. Hadden PW, Gerneke DA, McGhee CN, Zhang J. Skeletal elements of the penguin eye and their functional and phylogenetic implications (Aves: Sphenisciformes: Spheniscidae). Journal of Morphology. 2021;282(6):874-86. [PMID: 33786885] [PMCID: PMC8252517] [DOI]
22. Zehtabvar O, Masoudifard M, Ekim O, Ghorbani F, Davudypoor S, Memarian I, et al. Anatomical study of the scleral ring and eyeball of the long-eared owl (Asio otus) with anatomical methods and diagnostic imaging techniques. Veterinary Medicine and Science. 2022;8(4):1735-49. [PMID: 35506884] [PMCID: PMC9297753] [DOI]